water

MDPI

Article

Is the Groundwater in the Hunshandake Desert (Northern China) of Fossil or Meteoric Water Origin? Isotopic and Hydrogeochemical Evidence

Bing-Qi Zhu [1,*], Xiao-Zong Ren [2] and Patrick Rioual [3]

[1] Key Laboratory of Water Cycle and Related Land Surface Processes, Institute of Geographic Sciences and Natural Resources Research, Chinese Academy of Sciences, Beijing 100101, China
[2] School of Geography Science, Taiyuan Normal University, Jinzhong 030319, China
[3] Key Laboratory of Cenozoic Geology and Environment, Institute of Geology and Geophysics, Chinese Academy of Sciences, Beijing 100029, China
* Correspondence: zhubingqi@igsnrr.ac.cn; Tel.: +86-10-6488-9333

Received: 23 August 2018; Accepted: 19 October 2018; Published: 25 October 2018

Abstract: To gain an insight into the origin of groundwater in the Hunshandake Desert (HSDK), stable and radioactive isotopes and the major ion hydrochemistry of groundwater, as well as other natural waters, were investigated in this desert. The results showed that the groundwaters in the HSDK are freshwater (total dissolved solid (TDS) < 700 mg/L) and are depleted in δ^2H and $\delta^{18}O$ when compared with the modern precipitation. The major water types are the Ca–HCO_3 and Ca/Mg–SO_4 waters. No Cl-type and Na-type waters occurred in the study area. The ionic and depleted stable isotopic signals in groundwater, as well as the high values of tritium contents (5–25 TU), indicate that the groundwaters studied here are young but not of fossil and meteoric water origin, i.e., out of control by the modern and palaeo-direct recharge. A clear difference in the isotopic signals are observed between the groundwaters in the north and south parts of the study area, but the signals are similar between the groundwaters in the north HSDK catchment and its neighboring catchment, the Dali Basin. The topographical elevation decreases from the south (1396 m a.s.l.) to the north (1317 m a.s.l.) and the Dali (1226 m a.s.l.). Groundwaters in the north are characterized by lower chloride and TDS concentrations, higher tritium contents, higher deuterium excess, and more depleted values of δ^2H and $\delta^{18}O$ than those in the south. The spatial distribution pattern of these environmental parameters indicates a discrepancy between the hydraulic gradient of groundwater and the isotopic and hydrochemical gradients of groundwater in the HSDK, suggesting different recharge sources between the two parts in the desert. A combined analysis using the isotopic and physiochemical data of natural waters collected from the Dali Basin and the surrounding mountains was performed to investigate this problem. It indicates that groundwaters in the HSDK Desert are recharged from remote mountain areas (about 150–200 km to the east and southeast) but not from the north neighboring catchment.

Keywords: groundwater recharge; stable and radioactive isotope; ion geochemistry; fossil water; precipitation; middle-latitude desert

1. Introduction

From a global perspective, the International Atomic Energy Agency (IAEA, Vienna, Austria) estimates that much of the groundwater being developed in (semi-) arid regions is fossil water and is not sustainable. Thus, an appropriate management of these aquifers to meet human and ecosystem needs will require accurate estimates of groundwater recharge.

A correct estimate of the natural recharge of groundwater resources in arid environments has a key issue about whether the groundwater is younger or older [1–6]. The reason for this is that on the one hand, modern groundwater is more renewable than older "fossil" groundwater as water resources [1] but it is more vulnerable to industrial or agricultural contamination, as well as land-use changes at and near the surface of the Earth [7]. On the other hand, it is more strongly coupled and actively interactive with the broader hydrologic cycle, climate [8], and oceans [9].

The total recharge to groundwater is usually constituted by three main components, i.e., direct recharge, indirect recharge, and localized recharge. Water infiltration of atmospheric precipitation through the unsaturated zone to the groundwater is hydrologically defined as direct recharge [10]. In contrast, indirect recharge results from the percolation of a part of runoff water from the remote area through the streambeds or other channels and localized recharge refers to concentrated recharge by preferential flow through cracks, joints, and fissures [11]. The relative proportions of these components fluctuate according to climatic conditions, geomorphology, and geology. In arid regions, the most important mechanism of groundwater recharge is considered to be the infiltration from floods through the alluvial beds of ephemeral streams in wadi channels [12]. This is indirect recharge correlating with the above-given classification. Except in karst hydrology, up to now, there are only a few examples in the literature of the assessment of indirect recharge from a stream [12]. The assessment and regional consequences of indirect recharge constitute two challenges for future research on recharge [13]. This is especially challenging when this component highly fluctuates with time and space in the case of an ephemeral stream on a heterogeneous aquifer.

The Hunshandake Desert (HSDK) is one of the largest desert lands in the geographical center of the northeastern Asian Continent. There is abundant groundwater in this desert land and even rivers originate there due to the spillover of spring water, such as the tributaries of the Xilamulun River in its north and the Shandian River in its south (Figure 1). However, few datums on the groundwater recharge and its origin are available in the literature. In particular, whether the groundwater in the HSDK Desert is fossil water or meteoric water origin is not known. In this study, we investigate in detail the stable (H–O) and radioactive isotopic and hydrogeochemical composition of local precipitation, river water, lake water, spring water and groundwater in the HSDK Desert and surrounding areas. The aim of the investigations is to answer the following question: Groundwater in the HSDK Desert originates from fossil water or meteoric water?

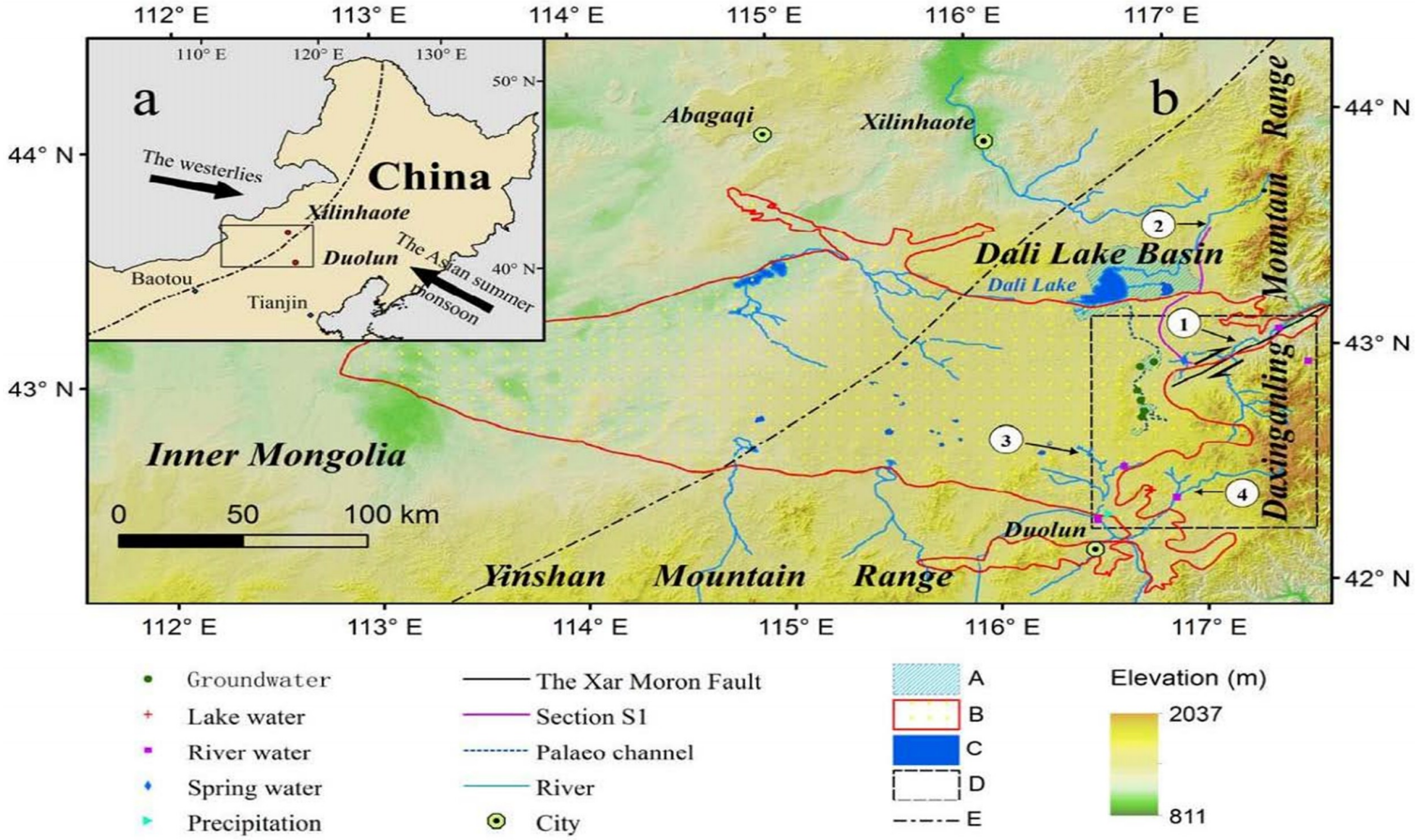

Figure 1. The Geographical location of the Hunshandake (HSDK) Desert in northern China. (**a**) The study area shown at a larger scale, and (**b**) the study area shown at a smaller scale, with detailed information about the boundary and tectonic settings of the desert land. A, the palaeo-lake area of the megalake Dali; B, the boundary of the HSDK; C, the modern lake area; D, the boundary of the sampling area; E, the boundary between the westerlies and the East Asian Summer Monsoon (EASM) climate systems. ①, the Xilamulun River. ②, the Gonggeer River. ③, the Shepi River. ④, the Tuligen River. The boundary between the westerlies and the EASM in (**a**,**b**) is modified from Reference [14]. The palaeo-lake area of the megalake Dali and the palaeo-channel (**b**) is modified from Reference [15]. The location of the Xar Moron Fault is referenced from Reference [16]. Section S1 is an elevation section starting from the upstream of the Dali Lake and ending with a spring sample (s2) in the riverhead of the Xilamulun River.

2. Regional Settings

2.1. Location and Landscape

The HSDK Desert (~21,400 km^2) is located as shown in Figure 1 and belongs to a climate-sensitive zone near the middle-latitude boundary of the semi-humid and semiarid, arid climate in northeastern China. Compared with the loess-desert transition zones of northwestern China, the HSDK is much closer to the ocean, and the East Asian summer monsoon (EASM) had a much stronger influence on this area [17,18]. The HSDK Desert belongs to the agro-pastoral ecotone in Inner Mongolia of China. Sandy fields in this area are primarily characterized by stabilized low-lying anchored dunes. The typical steppe covers more than half of the areas, while forest, shrub, farmland, and others are scattered in the remainder. Desertification has become the most severe issue since the late Holocene for these sandy lands due to the continental climate, sparse vegetation, sandy soils, and lack of water resources [19]. The terrain of the HSDK Desert is less rough and elevations decrease from ca. 1300 m a.s.l. in the southeast to ca. 1000 m a.s.l. in the northwest. Over the larger part of this desert, the ground cover consists of fixed and semi-fixed sandy dunes, with a few mobile dunes in areas of little vegetation. The dominated dune types are represented from parabolic to barchans, linear and grid-formed types, ranging from a few meters to over 40 m in height [20,21].

2.2. Structural and Geological Setting

Tectonically, the HSDK Desert is located at the central part of the Inner-Mongolia-Daxing'Anling Orogenic Belt (IMDOB), which is situated at the southeastern margin of the Central Asian Orogenic Belt (CAOB) (Figure 2) and is a key area characterized by the Paleozoic tectonic evolution of the CAOB [22,23]. The IMDOB is broadly subdivisible into five ENE–WSW–trending tectonic zones in Inner Mongolia, with the Solonker suture zone as its central part (Figure 2b).

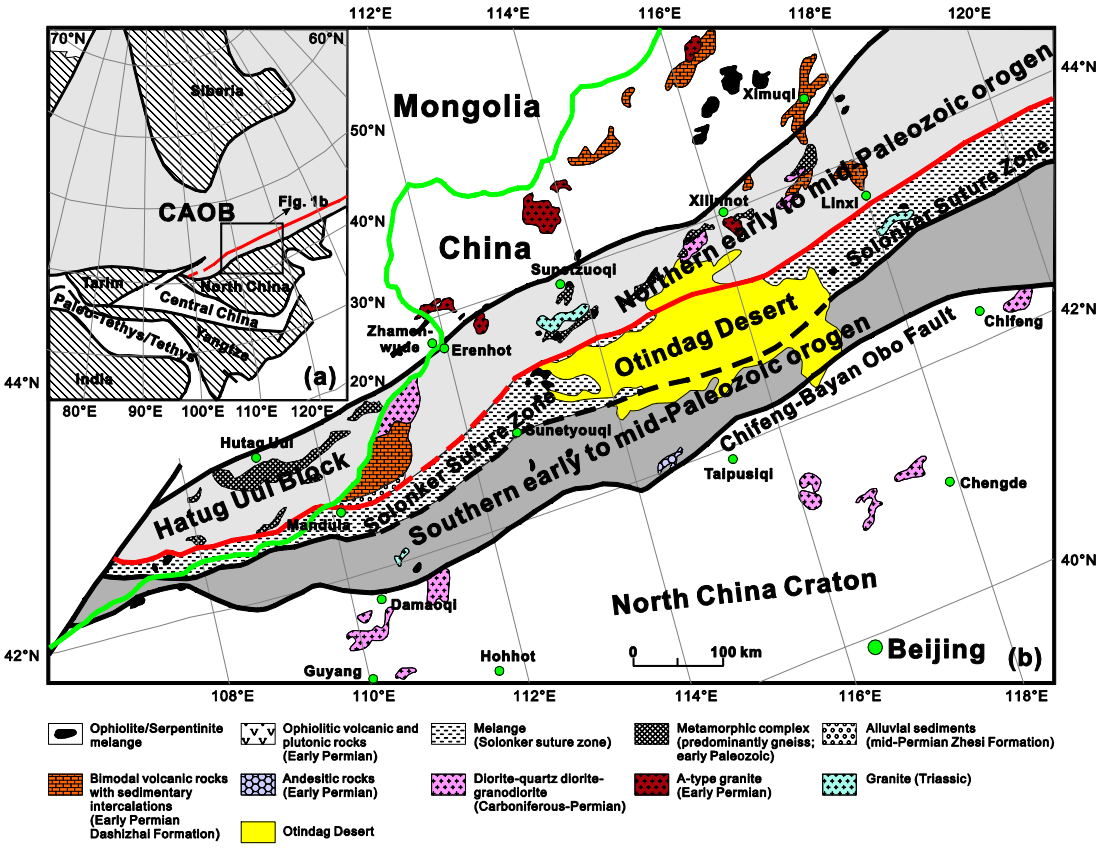

Figure 2. (**a**) The tectonic framework of the north China-Mongolian segment of the Central Asian

Orogenic Belt (CAOB, modified after Reference [24]). (**b**) Geological sketch map of the northern China-Mongolia tract (modified after Reference [22]). Note that the red line marks the early Permian palaeobiogeographical boundary [25,26], which coincides with the northern boundary of the suture zone. The green line in this figure represents the China/Mongolia border; dark gray: Southern orogen (early to mid-Paleozoic); light gray: Northern orogen (early to mid-Paleozoic) and the Hutag Uul Block. Inset Figure 1a shows the tectonic framework of Asia (after Reference [26]), in which principal cratons (Siberia, Tarim, North China, Yangtze, and India), orogens (CAOB, Central China and belts in Paleo-Tethys/Tethys), the Solonker suture (red line) and the position of Figure 1b are shown.

The Solonker suture zone (or Otindag block), where the HSDK Desert is located, represents a major paleo-plate boundary in Asia that stretches northeastwards over 2500 km in Mongolia and China [26]. The Solonker suture zone also represents the tectonic boundary between the northern (Hutag Uul Block-Northern orogen) and the southern (southern orogen-Northern margin of North China craton) continental blocks. The entire HSDK Desert is thus situated in a tectonic depression of the central Solonker suture zone with a few faults stretching east and west, such as the Xar Moron (Xilamulun) Fault in the east and the Chifeng-Bayan Obo Fault in the south. The desert is also marked by a series of lake basins in its northern margin along a branch fault of the Xilumulun Fault. Tertiary and Quaternary sandstones and mudstones are the common basement rocks under the dunes, and extensive volcanic basalts forming flat terrains are to the north [20,27].

2.3. Climate and Hydrogeology

According to the Koppen–Geiger climatic classification system [28], the HSDK Desert belongs to the snow climate, characterized by a warm summer, with precipitation transported by the EASM, and by a cold and dry winter under the influence of the East Asian Winter Monsoon (EAWM). The mean monthly temperature is −17.2 °C in January and 19.4 °C in July, and the mean annual temperature (MAT) is 2.26 °C [29]. The mean annual precipitation (MAP) is 359.6 mm, with July being the wettest month when precipitation reaches 96.7 mm. The annual evaporation is about 1936 mm [30], which results in high salinity (~5%) and a pH of ~9.79 (26.4 °C) of lake water in the west HSDK Desert.

The HSDK Desert depends on several water-bearing formations and units (aquifers) for their groundwater resources (Figure 3). Coarse- to fine-grained sedimentary rocks, magmatic rocks and metamorphic rocks of the IMDOB [23] form the major regional aquifer unit (Figure 3). The aquifer is generally unconfined in the dune fields of the HSDK Desert, unconfined to semi-confined in the Yinshan Mountains' Piedmont, and semi-confined to confined in the Daxing'Anling uplands (Figure 3). Local granular aquifers in the central desert are composed of coarse fluvial, lacustrine, and aeolian sediments, but their extent and thickness vary throughout the watershed [20,27]. The generally coarse-grained texture of the unconsolidated rock formations provides primary porosity in terms of groundwater flow in the desert.

The HSDK's groundwater table is only 1–3 m deep in the east part with water quality suitable for drinking [21], but much less available in the west. Regional water-level measurement in June 2010 indicated that the general depth of unconfined groundwater level ranges between 10 to 70 m from the ground in the HSDK Desert (Figure 3). At present no rivers flow into the HSDK Desert. Two rivers run through the eastern margins of the HSDK from west to east, i.e., the Xilamulun River in the north and the Shandian River and its two tributaries, the Shepi River and Tuligen River in the south. Both stem from the eastern and southeastern parts of the HSDK Desert and are recharged by local spring waters (Figure 1). The Xilamulun River flows to the east and finally goes into the Xiliao River, with a catchment area of 32.54×10^3 km^2 and an annual mean runoff of 6.58×10^8 m^3 [31]. The Shandian River is the upper reach of the Luan River, with a length of 254 km and a catchment area of 4.11×10^3 km^2 [32].

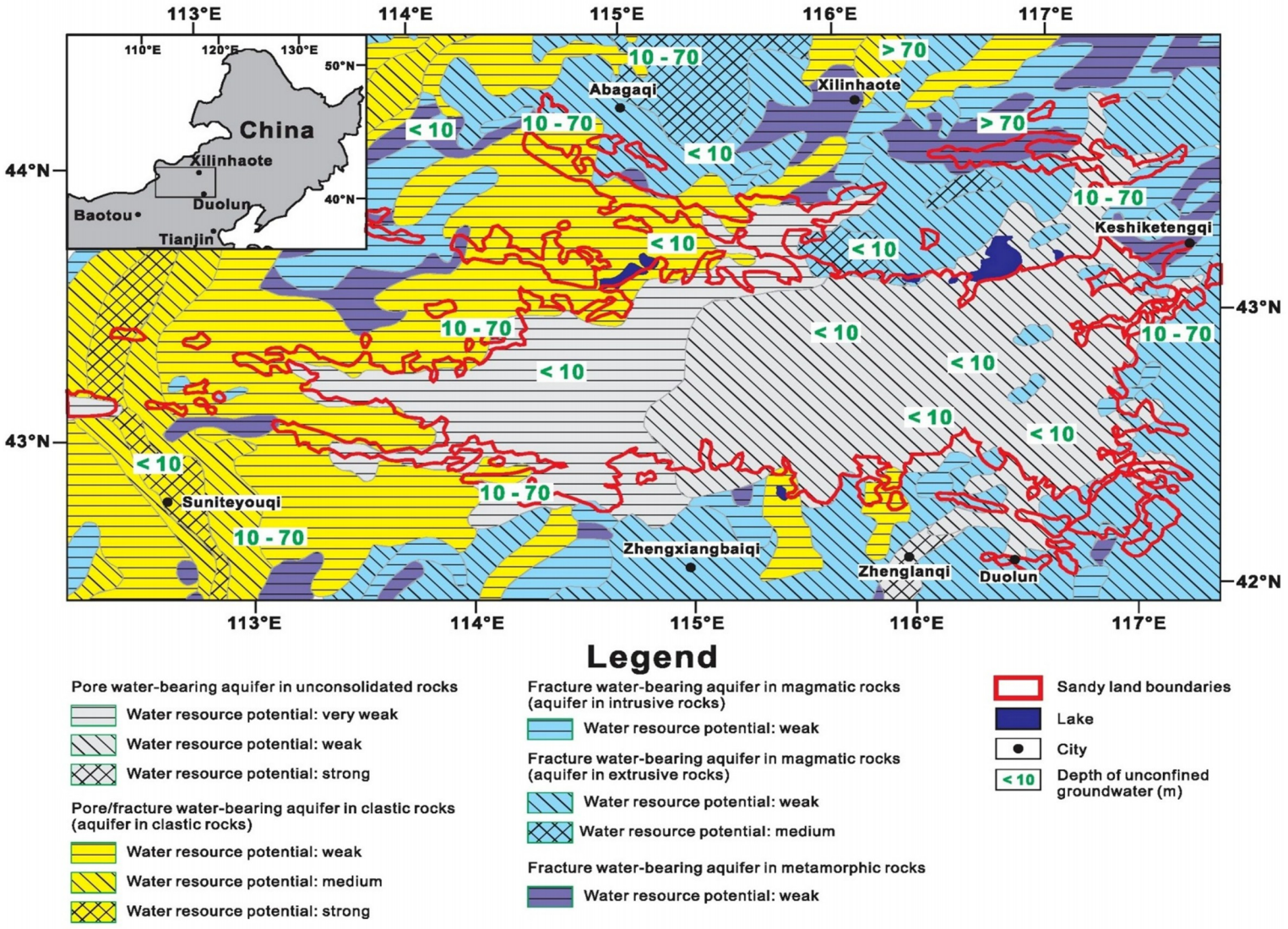

Figure 3. The hydrogeological division map of the HSDK Desert.

3. Methods

Up to now, no investigation at the Ontindag Desert was undertaken in order to study the groundwater recharge. In most cases carried out in the desert land, the sampled groundwater cannot be assumed to have been a portion of water moving unaltered from the point of recharge to the point where it is sampled. Instead, the sample is a mixture of waters with a wide range of transit times through the unsaturated and saturated zones. Consequently, multiple kinds of natural water samples need to be considered to trace the origin of groundwater in the HSDK Desert.

Fieldworks took place during the summer season of 2011 and the spring season of 2012. The water samples collected included groundwater, river water, lake water, spring water, and precipitation water. Groundwater was mainly retrieved from shallow and deep wells located over a wide area in dune fields of the study region. The surface waters were mainly sampled from rivers and lakes in the HSDK. The spring waters were collected from the riverhead of the Xilamulun River, the Shepi River, and the Tuligen Rivers as spillover water of groundwater in some depressions. One rainfall sample of the local atmospheric precipitation (p1) was collected at the southeastern margin of the HSDK in the 2011 summer season. Water samples for anions, stable, and radioactive isotope analysis were immediately filtered in the field using 0.45 mm Millipore MF filters (Merck, Darmstadt, Germany) and stored in 1000 mL double-stoppered polyethylene bottles, without air bubbles and protected from light. Water samples were filtered and acidified with 1% HNO_3 for cation analysis. Water samples were labeled and immediately stored in a freezer. They were sent to different laboratories as soon as possible to prevent chemical reactions until the analysis.

Water temperature, pH, oxidation-reduction potential (Eh), electrical conductivity (EC), total dissolved solids (TDS), and other chemical determinations (such as redox conditions and dissolved oxygen) were performed in the field. Variables were measured on site with a portable instrument (Eijkelkamp, Giesbeek, The Netherlands). The measurement errors were $<\pm 0.1$ °C for temperature, $<\pm 1\%$ for pH, $<\pm 5\%$ for Eh, $<\pm 5\%$ for EC, and $<\pm 0.5\%$ for TDS. The concentrations of major anions (F^-, Cl^-, $NO_2{}^-$, $NO_3{}^-$, $SO_4{}^{2-}$, and $H_2PO_4{}^-$) and cations (Li^+, Na^+, $NH_4{}^+$, K^+, Mg^{2+}, and Ca^{2+}) were determined by electrochemical detectors of an ion chromatography (Dionex 600, Dionex, Sunnyvale, CA, USA) in the Institute of Geology and Geophysics, Chinese Academy of Sciences, with measurement errors $<\pm 3\%$ for anions and $<\pm 2\%$ for cations. The concentrations of carbonate (alkaline) ions of $HCO_3{}^-$ and $CO_3{}^{2-}$ were measured by titrations with HCl (0.1 M) following the Gran Method [33], with an error $<\pm 5\%$. Two stable isotopes of ^2H and ^{18}O, expressed in δ-notation ($\delta^2H = {}^2H/{}^1H$, $\delta^{18}O = {}^{18}O/{}^{16}O$, in per mil (‰) after normalization to VSMOW scale) relative to the Vienna standard mean water (VSMOW), were measured using a MAT-252 (Finnigan Mat, Bremen, Germany) in the Laboratory for Stable Isotope Geochemistry, Institute of Geology and Geophysics, Chinese Academy of Sciences, with σ (standard deviation) $< \pm 0.374‰$ and $<\pm 0.062‰$ for δ^2H and $\delta^{18}O$, respectively.

Seven groundwater samples (500 mL each), collected from wells (6–60 m deep) in the study area, were prepared for the analysis of a radioactive isotope (tritium) (Table 1). A detailed analytical method can be seen from Reference [15]. The measurement errors are $<\pm 3\%$. The analytical data of the physiochemical parameters and the stable and radioactive isotopes of the water samples collected in this study are listed in Tables S1 and S2 (online supplementary Tables S1 and S2) and Table 1, respectively. The study area and the location for each sample analyzed are showed in Figures 1 and 4, respectively.

Table 1. The analytical data of stable and radioactive isotopes measured for the water samples in this study. / = not detected.

Sample ID	Water Type	δ^2H (‰)	σ‰	$\delta^{18}O$ (‰)	σ‰	Deuterium Excess (d)	Tritium (^3H) (TU)
g1	groundwater	−66.764	0.199	−8.895	0.026	4.496	/
g2	groundwater	−64.758	0.291	−9.336	0.039	9.930	/
g3	groundwater	−63.424	0.269	−8.635	0.008	5.656	/
g4	groundwater	−66.055	0.149	−9.621	0.062	10.913	7.25
g5	groundwater	−65.462	0.111	−9.802	0.027	12.954	9.98
g6	groundwater	−68.913	0.287	−10.514	0.039	15.199	22.9
g7	groundwater	−73.105	0.298	−10.662	0.041	12.191	/
g8	groundwater	−73.676	0.220	−11.023	0.037	14.508	19.6
g9	groundwater	−72.530	0.181	−11.041	0.015	15.798	24.3
g10	groundwater	−74.362	0.201	−11.127	0.026	14.654	18.7
g11	groundwater	−75.924	0.340	−11.260	0.015	14.156	1.86
l1	lake water	−53.128	0.229	−6.553	0.002	−0.704	/
l2	lake water	−50.721	0.304	−6.320	0.026	−0.161	/
l3	lake water	−42.877	0.239	−4.292	0.034	−8.545	/
l4	lake water	−34.155	0.243	0.381	0.040	−37.203	/
l5	lake water	−45.057	0.206	−4.987	0.009	−5.161	/
l6	lake water	−52.866	0.187	−6.150	0.049	−3.666	/
r1	river water	−66.157	0.118	−10.069	0.015	14.395	/
r2	river water	−64.996	0.148	−9.549	0.012	11.396	/
r3	river water	−73.790	0.315	−11.083	0.021	14.874	/
r4	river water	−85.155	0.244	−11.781	0.005	9.093	/
r5	river water	−74.978	0.195	−10.084	0.003	5.694	/
s1	spring water	−70.832	0.074	−10.340	0.007	11.888	/
s2	spring water	−72.601	0.281	−10.468	0.046	11.143	/
p1	rain water	−47.435	0.374	−7.141	0.017	9.693	/

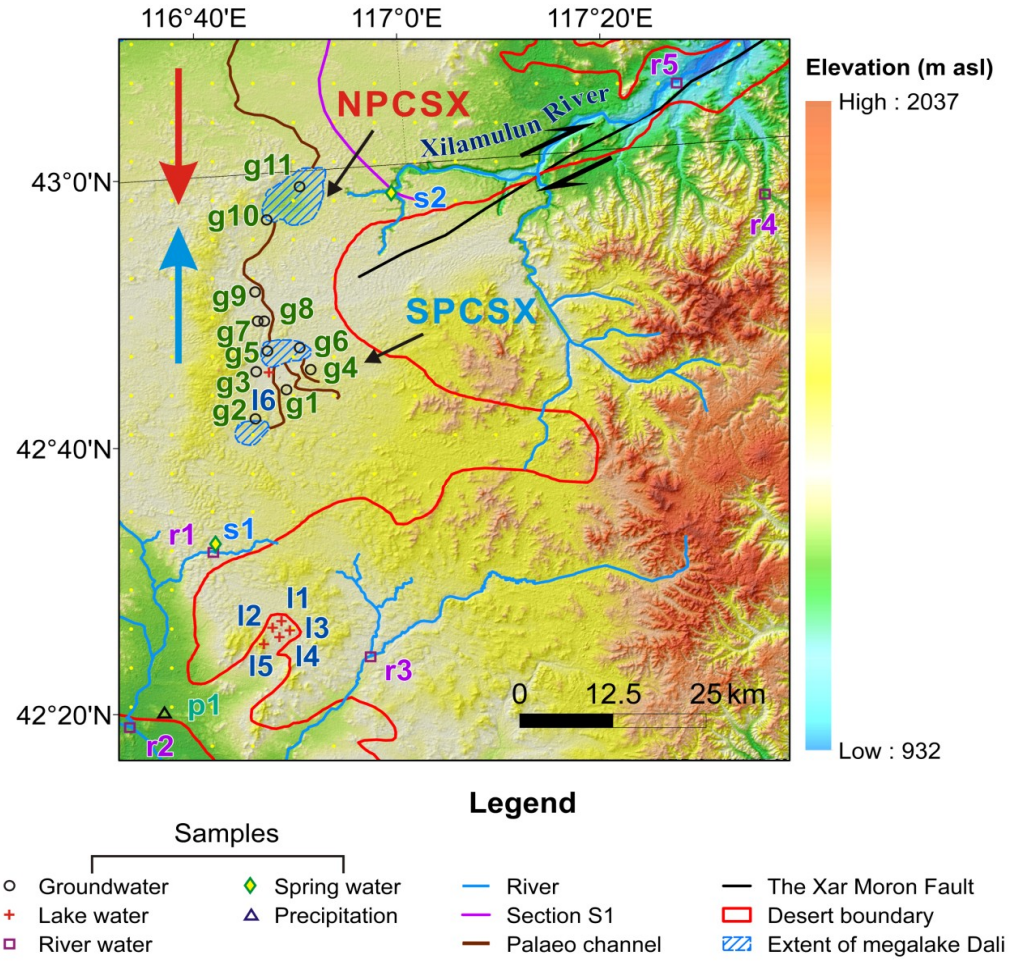

Figure 4. The locations of the water sampling sites in this study.

4. Results

The pH values of the water samples studied varied from 6.26 to 9.44 (except sample p1, precipitation, 4.61) (Table S1) with a mean value of 7.27, indicating that the waters are generally neutral to slightly alkaline. The TDS ranged between 67 and 660 mg/L (average 211 mg/L) (Table S1), thus, all belonging to fresh water (TDS < 1000 mg/L) in the salination classification of natural water [34].

The variations in ion concentrations of the major cations and anions in the studied water samples were displayed in a Schoeller diagram [35] (Figure 5). In general, the groundwater samples had the highest concentrations of cations and anions while the rainfall sample (p1) had the lowest concentrations, and the lake, river, and spring waters had intermediate values. The calcium concentration was the highest among cations in almost all of the water samples, and the alkalinity was the highest among anions in most of the water samples, except for several groundwater samples (g3, g4, g5, g6, and g11) and one of the spring samples (s1) and the precipitation samples (p1), which had higher SO_4 concentrations than alkalinity (Figure 5).

The water samples studied can be classified into two water types in the Piper diagram (Figure 6). Type I, the Ca–HCO_3 water, which generally represents the typical bicarbonate water affected by near-surface mineral weathering, and type II, the Ca/Mg–SO_4 water, which indicates saline water dominated by alkaline earth metals [36–38]. For water type I, the weak acids exceeded the strong acids; the carbonate hardness (secondary alkalinity) exceeded 50% and was dominated by the alkaline earths. While for water Type II, the strong acids exceeded the weak acids and no carbonate hardness exceeded 50%. The alkaline earth metals (Ca + Mg) exceeded the alkalis (Na + K) in all the water samples studied. No Cl-type and Na-type waters occur in the study area (Figure 6), indicating a primary stage of water evolution for natural waters in the HSDK, in terms of the hydrogeochemical perspective.

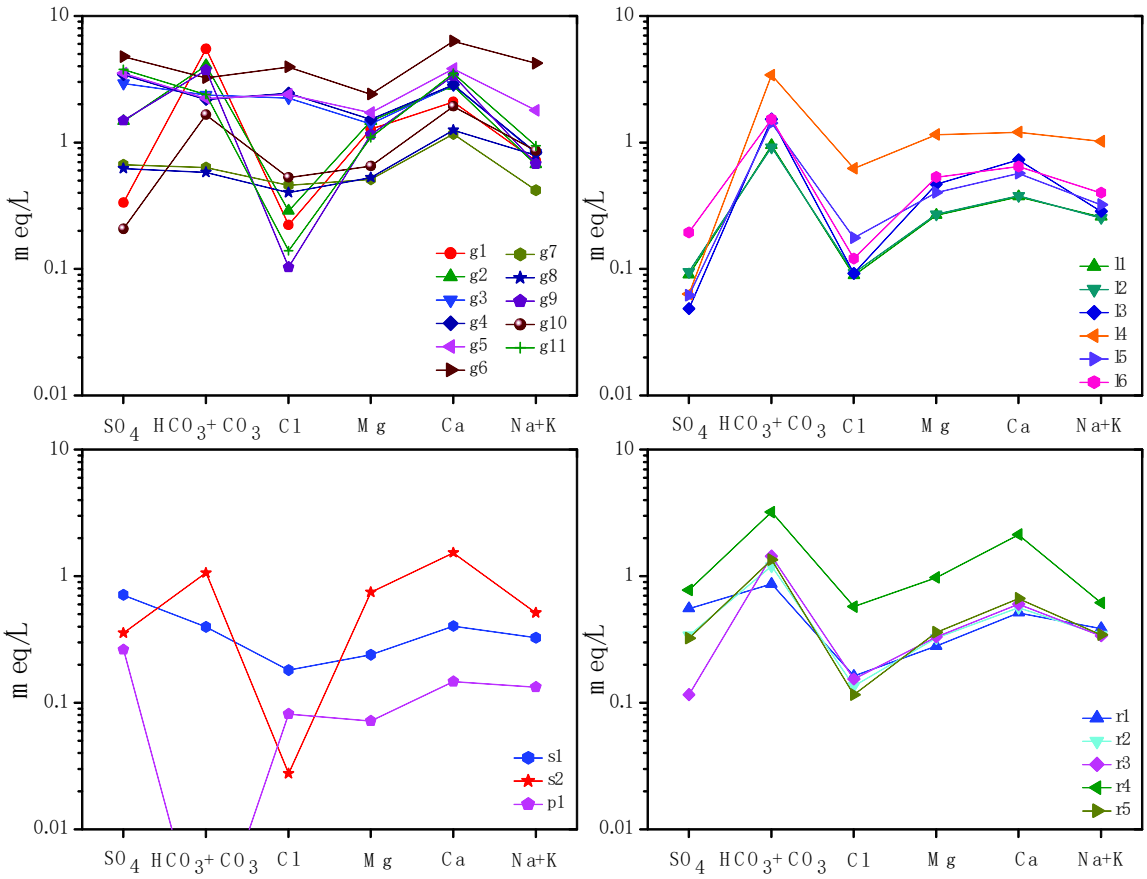

Figure 5. The Schoeller diagram [35]. The HCO_3 + CO_3 concentration in sample p1 was not shown due to its value being lower than the detection limit.

The δ^2H values of the groundwater samples collected in this study varied from −63.42‰ to −75.92‰ (Table 1), with an average of −69.53‰. The $\delta^{18}O$ values ranged between −8.64‰ and −11.26‰ (Table 1), with an average of −10.17‰. The spring water samples were relatively concentrated in δ^2H and $\delta^{18}O$ and were greatly similar to those of the groundwater sample (Figure 7). The δ^2H and $\delta^{18}O$ values in the spring samples varied from −70.83‰ to −72.60‰ (mean value of −71.72‰) and from −10.34‰ to −10.47‰ (mean value of −10.40‰), respectively (Table 1).

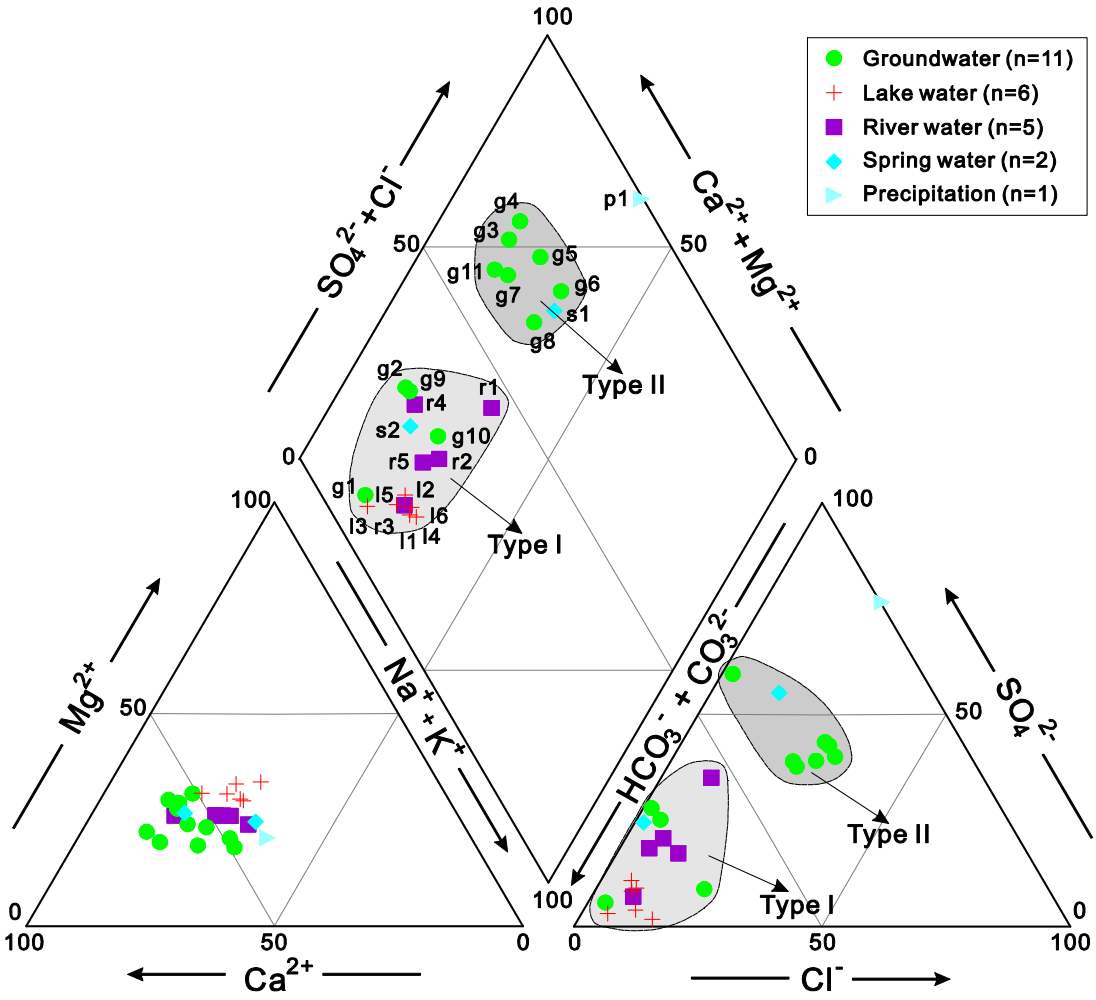

Figure 6. The Piper diagram [39] showing the relative abundances of major cations and anions in the studied water samples. Major water types are also shown.

The δ^2H and $\delta^{18}O$ values in the river water samples were slightly more variable and were also similar to those of the groundwater (Figure 7), with a range between −65.00‰ and −85.16‰ (mean value of −73.02‰) in δ^2H values and a range between −9.55‰ and −11.78‰ (mean value of −10.51‰) in $\delta^{18}O$ (Table 1). The lake water samples were enriched in δ^2H and $\delta^{18}O$ by comparison to the groundwater samples (Figure 7), with a range between −34.16‰ and −53.13‰ (mean value of −46.47‰) in δ^2H values and a range between 0.38‰ and −6.55‰ (mean value of −4.65‰) in $\delta^{18}O$ (Table 1). The precipitation sample p1 showed a δ^2H value of −47.4‰ and a $\delta^{18}O$ value of −7.14‰ (Table 1).

The isotopic regression equation of the HSDK evaporation line (EL1) (Figure 7), which was calculated based on the δ^2H and $\delta^{18}O$ data of the groundwater, lake, river, and spring water samples in this study, was $\delta^2H = 4.09\ \delta^{18}O - 28.31$ ($R^2 = 0.93$, $n = 24$).

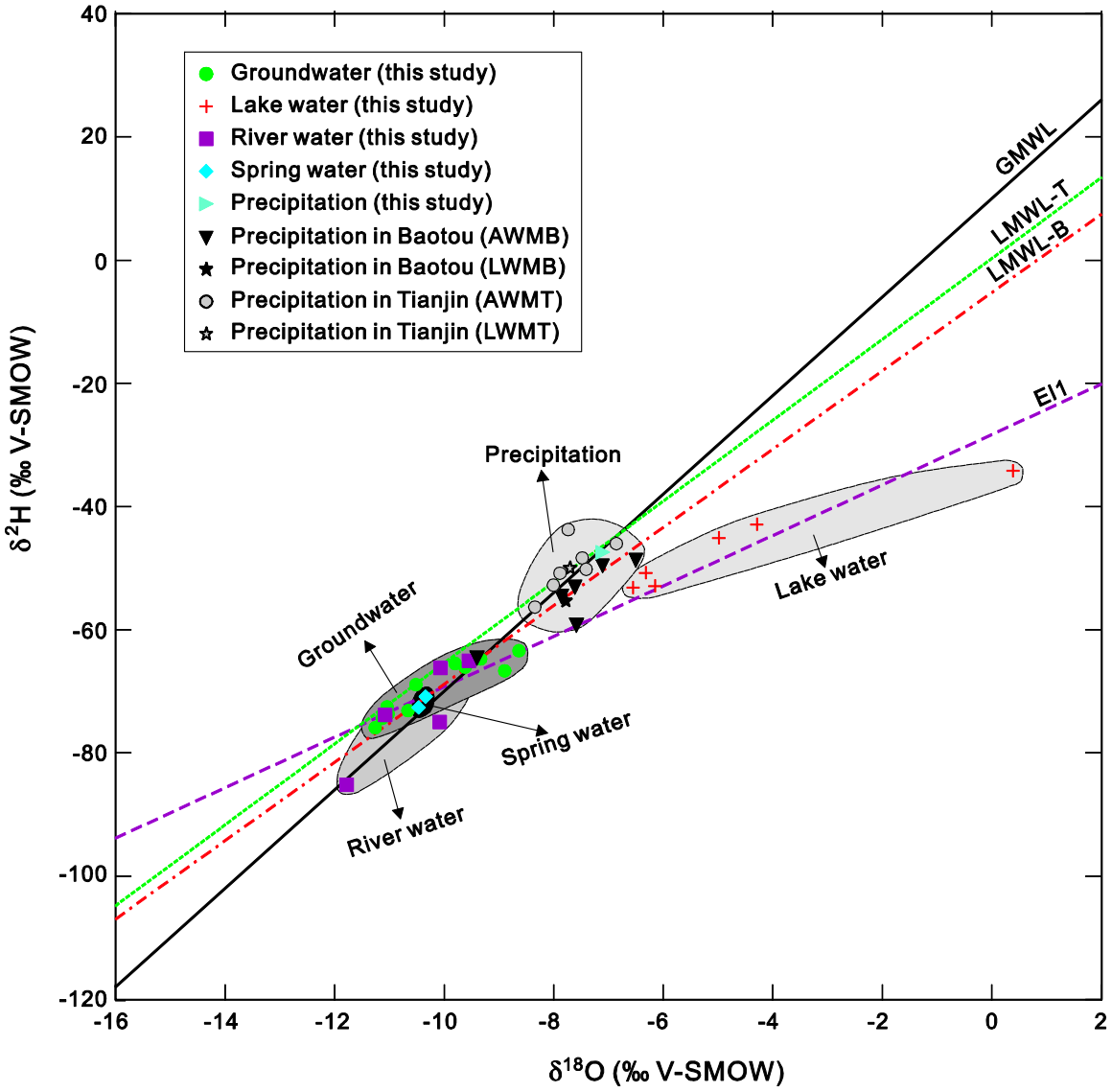

Figure 7. The bivariate diagram of δ^2H and δ^{18}O (in per mil (‰) after normalization to VSMOW scale). AWMB: annual weighted mean value at the Baotou station (calculated in this study); AWMT: annual weighted mean value at the Tianjin station (calculated in this study); LWMB: long-term weighted means at the Baotou station (calculated in this study); LWMT: long-term weighted means at the Tianjin station (calculated in this study); GMWL: Global Meteoric Water Line [40]; LMWL-B: local meteoric water line calculated based on the data from the Baotou station (calculated in this study); LMWL-T: local meteoric water line calculated based on the data from the Tianjin station (calculated in this study).

The content of the radioactive isotope of tritium (^{3}H) was measured in seven well groundwater samples with 6–60 m depth. The tritium concentrations ranged from 1.86 to 24.35 TU (Table 1), with an average of 14.95 TU, higher than the mean tritium concentration (9.8 TU) of groundwater in the Vienna Basin, Austria [41], the seat of the International Atomic Energy Agency (IAEA, Vienna, Austria).

5. Discussion

5.1. Meteoric Water Recharge from Modern Precipitation

In this study, the decadal isotope data (1981–2010) of atmospheric precipitation around the HSDK were used to determine the isotopic relationship between the local groundwater and the regional precipitation that is available from the IAEA Global Network of Isotopes in Precipitation (GNIP)

database. Two GNIP meteorological stations were chosen: the Baotou station, located to the southwest of the HSDK as representative of the western Asian summer monsoon system (ASMS), and the Tianjin station, located to the southeast of the HSDK, as representative of the eastern ASMS (Figure 1a). The historical isotopic data (^{3}H, δ^2H and δ^{18}O, ‰ VSMOW) over the last four decades from the two stations, as well as other data including the daily precipitation amount (mm) and air temperature (°C) in the same period, were taken as references for the stable isotopic signals in precipitation.

Compared to the precipitation data from the GNIP stations and from the local precipitation (p1), the groundwater samples were depleted in heavy stable isotopes (Figure 7). In comparison to the precipitation data, the water samples from springs and rivers in the study area also showed depletion characteristics in the stable isotopes of δ^2H and δ^{18}O (Figure 7). The regional meteoric water lines can be statistically expressed as the isotopic regression equation of $\delta^2H = 6.36\ \delta^{18}O - 5.21$ (line LMWL-B), based on the isotopic data from the Baotou station, and can be expressed as $\delta^2H = 6.57\ \delta^{18}O + 0.31$ (line LMWL-T), based on the data from the Tianjin station (Figure 7). Except for the lake water samples, most of the groundwater, river water, and spring water samples in the HSDK fall on or lie between the LMWL-B and the LMWL-T lines, and are located at the lower left area of the precipitation points (Figure 7). This indicates that no deep evaporation process was experienced by these ground and surface waters (except for lake waters), even less than the precipitation. For the HSDK evaporation line (EL1), its equation slope and intercept were significantly lower than that of the GMWL, LMWL-B, and LMWL-T (Figure 7).

Almost all the annual weighted mean values of the stable isotope contents in the precipitation at Baotou and Tianjin were enriched in δ^2H and δ^{18}O compared to those values measured for the groundwater, spring water, and river water samples in this study (Figure 7). Because the isotopic evolution of δ^2H vs. δ^{18}O in water illustrated in the Craig line represents a one-way and irreversible process, the water bodies distributed at the upper right area of the Craig line cannot be the recharge sources for the water bodies distributed at the lower left area of the line. Such results indicate that the groundwater, river water, and spring water in the HSDK are not recharged by the regional precipitation, namely, that no significant modern direct recharge has taken place for groundwater in the HSDK.

In addition to groundwater, the river and spring water samples from the HSDK had similar isotopic signals with those of groundwaters and also deviated from the modern regional precipitation in the Craig diagram (Figure 7). These water samples came from the Xilamulun, Shepi, and Tuligen rivers. They shared the same evaporation line (EL1) with the groundwater and lake water samples (Figure 7). Generally speaking, natural waters that have the same recharge source are distributed on the same line of evaporation in the δ^2 and δ^{18}O diagram [42]. This indicates that the recharge sources of groundwater, river water, spring water, and lake water in the HSDK are genetically associated and differ from the regional precipitation.

5.2. Meteoric Water Recharge from Winter Precipitation

Since the groundwater samples in the HSDK are depleted in their δ^2H and δ^{18}O values even more than those from modern rainfall (Figure 7), it can be deduced that they may be sourced from other waters characterized by similar or more depleted signals in their stable isotopic compositions.

Because the HSDK is under the control of the East Asian Summer Monsoon climate [43], the modern rainfall in the desert is mainly sourced from summer precipitation. The climatic characteristics are illustrated by the seasonal distributions in annual mean precipitation (Figure 8a), in annual mean air temperature (Figure 8b), and in annual mean water vapor pressure (Figure 8c) over the last forty years at the two surrounding GNIP weather stations in Baotou and Tianjin. These records indicate that summer rainfall is warmer and relatively positive in its signals of δ^2H and δ^{18}O by comparison with those of waters issued from colder environments. This is due to the effect of thermal fractionation or/and dynamic fractionation on isotopic fractionation [38]. Thus, it can be speculated that groundwater in the HSDK is derived from cold environments, namely cold water origin, such as

(1) modern precipitation in winter, (2) palaeowater formed in the past glacial period, or (3) mountains waters in colder and wetter conditions.

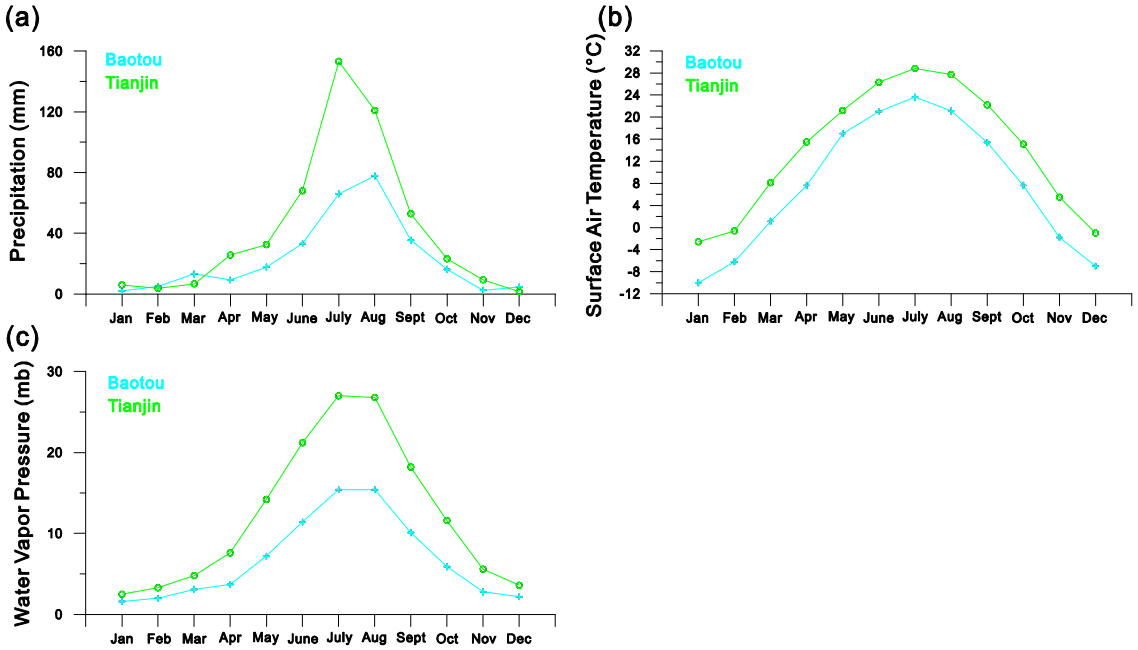

Figure 8. The seasonal mean distributions of precipitation (**a**) surface air temperature (**b**) and water vapor pressure (**c**) from the Baotou and Tianjin weather stations (station sites seen in Figure 1a) in the surrounding areas of the HSDK for the period 1981–2010.

With regard to the hypothesis (1) "the modern winter precipitation", we can get clues from the isotopic records of winter precipitation in the Baotou and Tianjing stations. It emerges that the annual mean values of δ^2H and $\delta^{18}O$ over the last forty years are more depleted in winter precipitation than in summer precipitation at the Baotou and Tianjin stations (Figure 9a,b). This suggests that regional winter precipitation qualifies to be a potential source of groundwaters in the HSDK. However, the limited amount of water derived from winter precipitation in these regions challenge the idea that this is an efficient source of groundwater. In fact, the precipitation amounts and the water vapor pressures (effective moisture) in winter months are much lower than those in the summer months at both the Baotou and Tianjin stations (Figure 8a,b), indicating that the winter seasons in these regions are relatively colder and drier but not colder and wetter. A colder-wetter winter season is a necessary condition for winter precipitation to be a water source for the formation of groundwater under a summer monsoon climate. This is because the bigger amounts of summer precipitation will easily remove or weaken the depleted isotopic signals of winter precipitation in groundwater.

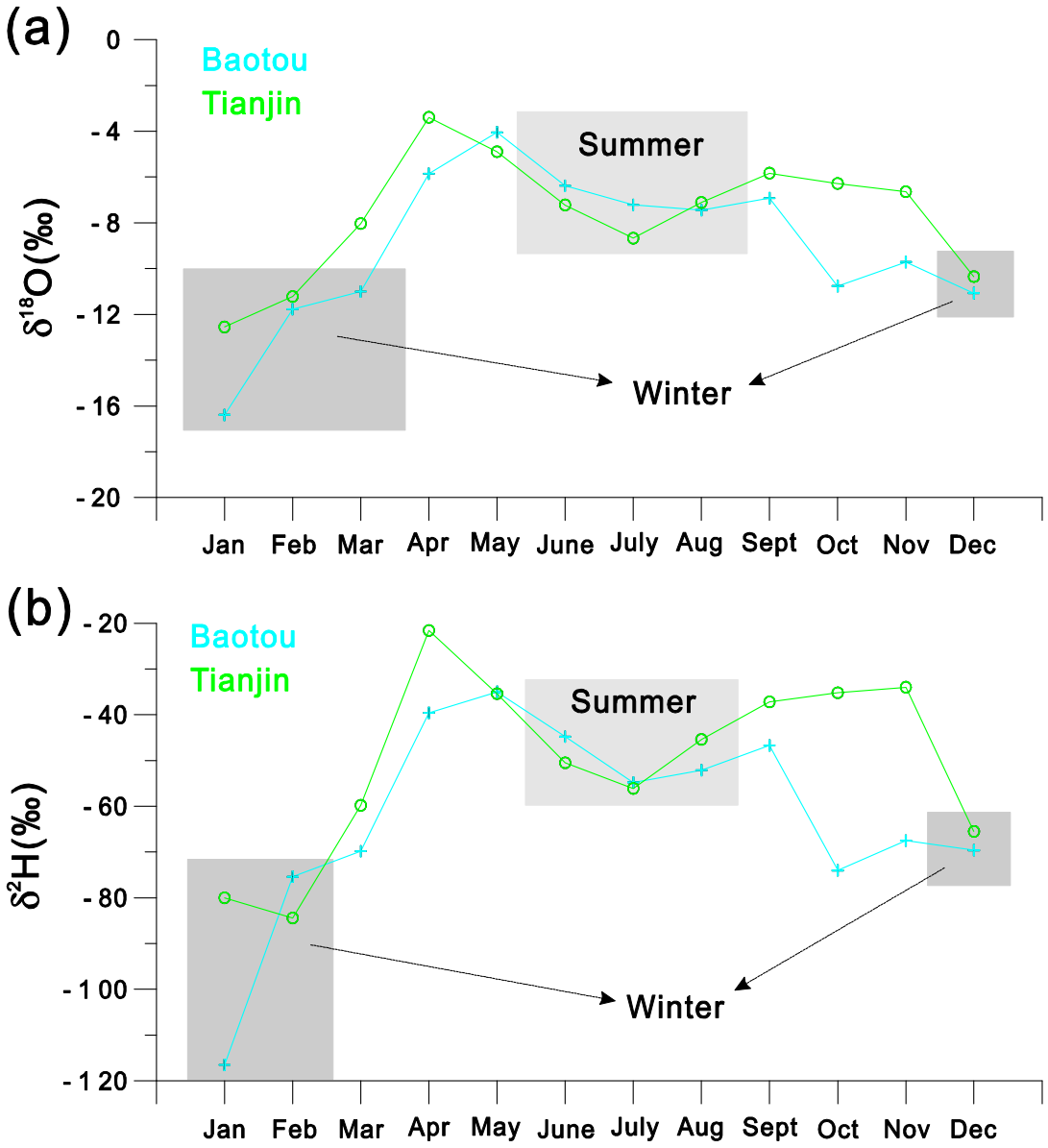

Figure 9. The seasonal mean distributions of $\delta^{18}O$ (**a**) and $\delta^{2}H$ (**b**) values in the precipitation from the Baotou and Tianjin weather stations in the surrounding areas of the HSDK for the period 1986–2001 (cited from the IAEA Global Network of Isotopes in Precipitation (GNIP) database).

5.3. Fossil Water Origin

The fossil water, such as the palaeowaters formed in colder and wetter periods like the last glacial, has been proposed to be a potential water source for groundwaters in the wide arid lands of the world. In fact, the depleted signals of stable isotopes ($\delta^{2}H$ and $\delta^{18}O$) in groundwater have been recognized in global arid and semi-arid regions, such as the Sinai Desert in Egypt [44], Israel [45], South Australia [46,47], Badanjilin Desert [48] and northern China [49], Atacama Desert [50], Saudi Arabia [51], and North Africa [52]. The signals are very often explained as palaeo-groundwater that recharged by precipitation during past wetter and colder periods [46,47,53]. Gat and Issar [44] reported that palaeowaters played a central role in the deep aquifers of the Sinai Desert, with the evidence that groundwater stable isotope compositions ($\delta^{18}O$ and $\delta^{2}H$) were more negative than those of weighted mean contemporary rainfall. Ma et al. [49] presented data from groundwater in the aquifer of Jinchang city and the adjacent Gobi desert areas in northern China, which showed that palaeowaters were depleted in ^{18}O and ^{2}H relative to modern precipitation in the same region.

In order to identify the role of palaeowater recharge on groundwater in the HSDK, we used the tritium data as an environmental tracer to estimate the groundwater age in the HSDK. The half-life of tritium is 12.43 years. Based on this decay time and the tritium concentrations in groundwater, the exponential decay equation can be used to provide a qualitative age to interpret the regional groundwater flow system [49]. Due to the lack of tritium data of local precipitation in the HSDK, we still used the tritium data at the GNIP stations of the Baotou and Tianjin as the background values in precipitation of recent years.

Based on the equation $N = N_0 e^{-\lambda t}$ [49] (where N = content of residual tritium in water sample, $\lambda = 0.0565$, the radioactive decay constant, N_0 = the content of tritium at the time of rainfall and t = years after precipitation), the residual tritium was theoretically calculated and the ages of groundwater samples (0–60 years) were established (Table 2). The result indicates that a recent recharge took place several decades after the peak in global nuclear tests. Taking into account the relatively high tritium contents and the calculated ages of the groundwater samples in this study (Table 2), we conclude that the groundwater is generally not older than 70 years in the study area. Thus, the hypothesis that groundwater in the HSDK is formed from fossil water formed during the last glacial period is not valid.

Table 2. The measured contents of tritium in the groundwater samples studied and the calculated ages of these samples. NM: not measured, NE: not estimated.

Sample-ID	Tritium Content (TU)	Possible Ages (Years)
g1	NM	NE
g2	NM	NE
g3	NM	NE
g4	7.25	20–40
g5	9.97	13–33
g6	22.91	0–20
g7	NM	NE
g8	19.61	0–20
g9	24.34	0–17
g10	18.68	0–22
g11	1.86	40–65

5.4. Recharge Sources from Neighboring Catchment

It is worth noting that the values for groundwater in the north part of the study area are more depleted in δ^2H and $\delta^{18}O$ than those in the south part (Table 1), suggesting that the groundwater might be potentially recharged by water resources coming from the northern neighboring catchment of the eastern HSDK, namely the Dali Basin. In order to estimate the potential linkage between the HSDK and Dali, recently published data of deuterium and oxygen-18 in groundwaters, lake waters, river waters, and spring waters sampled from the Dali Basin (e.g., [54,55] are compiled in this study and were co-analyzed with the data from the HSDK.

In total, about 70 natural water samples from the Dali and HSDK with δ^2H vs. $\delta^{18}O$ values are shown in Figure 10. All of these samples fell on or lied near the evaporation line EL2 in Figure 10, with a regression equation of $\delta^2H = 4.81\ \delta^{18}O - 21.55$ and a higher correlation coefficient ($R^2 = 0.98$, $n = 70$) than that of EL1 ($R^2 = 0.93$, $n = 24$) for the HSDK samples.

Compared to the groundwater samples in the HSDK, water samples from the groundwaters, rivers, and springs from the Dali Basin are more depleted in $\delta^{18}O$ and δ^2H (Figure 10). Such results further indicate that, in terms of its isotopic signature, the groundwater in HSDK has a close relationship with the natural waters in Dali, except for the lake water in Dali. It seems that the Dali water is a potential source for groundwater in the HSDK, or both of them are recharged by a common source derived from the surrounding mountains.

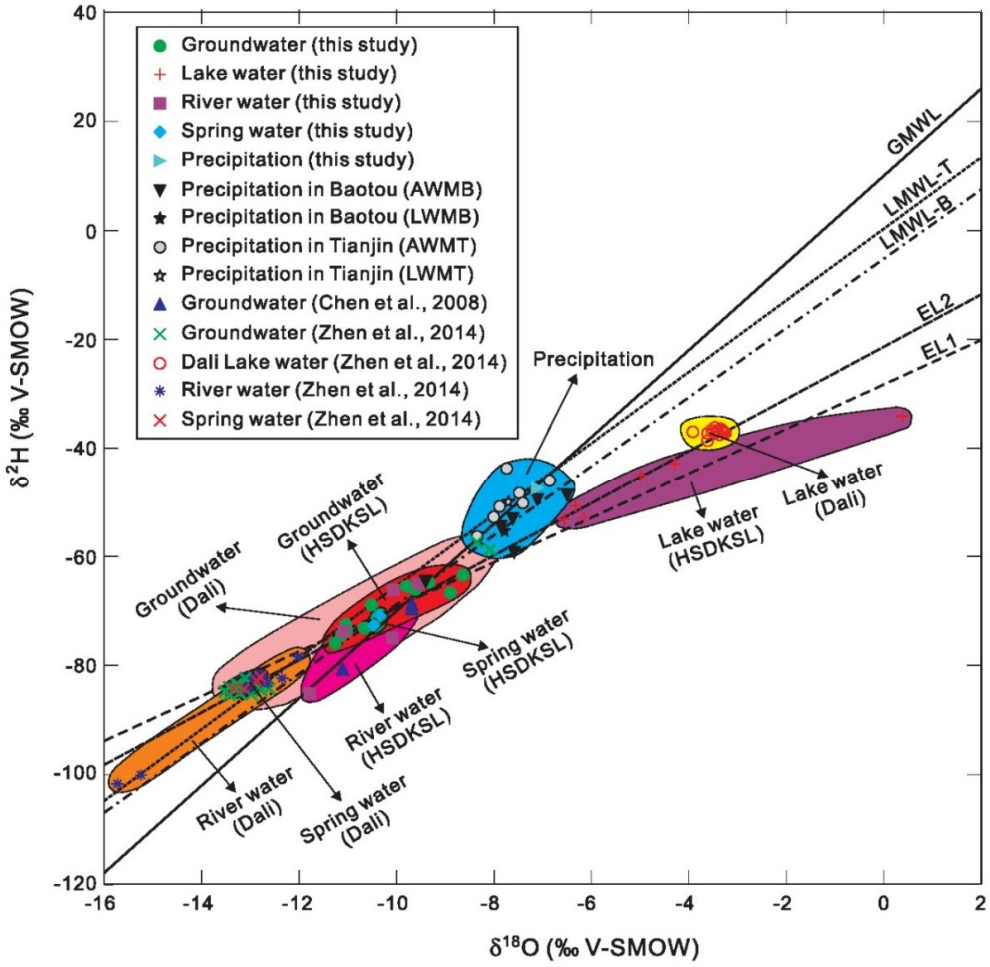

Figure 10. The bivariate diagram of δ^2H and $\delta^{18}O$ (in per mil (‰) after normalization to the VSMOW scale) for the natural water samples collected from the Dali Basin and from the study area. AWMB, AWMT, LWMB, LWMT, GMWL, LMWL-B, LMWL-T, and EL1 are the same as in Figure 7. EL2 evaporation line calculated based on the data from the groundwater, lake water, river water, and spring water samples in the HSDK and in the Dali Basin. The data for the Dali were taken from previous studies [54,55].

5.4.1. Recharge Source from the Dali River Water

The similar signals of deuterium and oxygen-18 between the HSDK groundwater and the Dali river water (Figure 10) point towards the idea that the groundwater in the HSDK might be sourced from the river water in the Dali Basin since the Dali has more depleted isotopic signals in water than the HSDK (Figure 10).

Considering the topographical gradient of elevations between the two regions, however, river water in the Dali Basin cannot flow into the eastern HSDK because the terrain elevation of the Dali Basin is lower than that of the HSDK (Figure 1). This is also the reason why the huge Dali Lake that lies in the Dali Basin has no equivalent in the HSDK (Figure 1). If there is a hydraulic linkage between the two regions, water should flow from the HSDK into the Dali, but not conversely.

In view of the hydraulic gradient, river water in the Dali Basin could not be a recharge source for groundwater in the HSDK. However, in view of the isotopic gradients, conversely, groundwater in the HSDK could not be the source of river water in the Dali at present, due to the more depleted values of deuterium and oxygen-18 in Dali than in HSDK (Figure 10). Thus, the similar isotopic signals between the river water in Dali and the groundwater in HSDK indicate that these waters might be recharged from a common source.

5.4.2. Recharge Source from the Dali Groundwater

Similar isotopic signals also occurred in the groundwaters between the HSDK and the Dali Basin (Figure 10). In order to understand the linkage of groundwaters between the two regions, the potential movement of groundwater in the transition zone of the two regions is discussed here.

In this study, a groundwater-sampling project was designed in the field along a N-S section of a palaeo-channel located at the transition zone between the Dali and HSDK (Figure 4). The channel is named "PCSX" in this study, with the north part of the channel as "NPCSX" and the south part as "SPCSX" (Figure 4).

Regarding the topographical gradient in the HSDK, the GPS elevation of the northernmost sampling site in the NPCSX (g11, about 1317 ± 3 m a.s.l.) was much lower than that of the southernmost site in the SPCSX (g1, 1396 ± 3 m a.s.l.) (Figure 4 and Table S1). There is a drop of about 80 m between the NPCSX and the SPCSX. Under such a slope, the underground hydraulic gradient for the groundwater flow can be roughly parallel with that of the surface water flow, namely that the groundwater flow should move downwards from the SPCSX area to the NPCSX area.

Compared the NPCSX and SPCSX regions, the stable isotopic values ($\delta^{18}O$ and $\delta^{2}H$) of groundwaters in the SPCSX region vary greatly with a large amplitude, while those in the NPCSX are relatively constant (Figure 11). This indicates that the recharge sources of groundwater in the SPCSX are more diverse than those in the NPCSX. The constant variations indicate that the recharge source of groundwater in the NPCSX is relatively unitary. The isotopic values in the SPCSX are much lighter than those in the NPCSX along the distance section from the south to north (Figure 11). The heaviest values occurred in the sample g11 collected from the NPCSX (Figure 11), indicating the water being firsthand recharged. The spring water sample s2, a representation of discharge water, is characterized by medium values of $\delta^{2}H$ and $\delta^{18}O$. Similarly, the deuterium excess values of these groundwaters also show such spatial patterns in the two regions (Figure 12). These results indicate that the groundwaters in the SPCSX area, with relatively enriched isotopic signals in $\delta^{2}H$ and $\delta^{18}O$ in comparison with those in the NPCSX area, which are composed of a mixture of the groundwaters in the NPCSX with other waters. In consequence, the spring water sample s2 in the discharge zone is characterized by an intermediate isotopic signal (Figures 11 and 12).

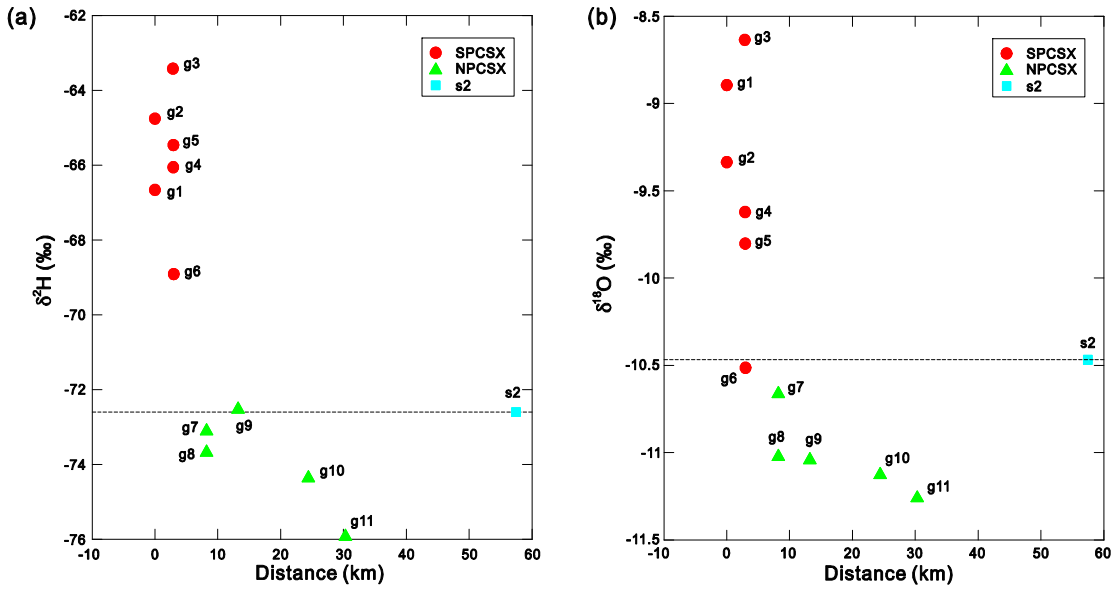

Figure 11. The variations of $\delta^{2}H$ (**a**) and $\delta^{18}O$ (**b**) in the groundwaters versus their distances away from the groundwater sample g1 along the palaeoriverchannel (PCSX) from the south to north. The dashed line represents the corresponding values of the spring water sample s2, and divides the samples into the NPCSX and the SPCSX parts.

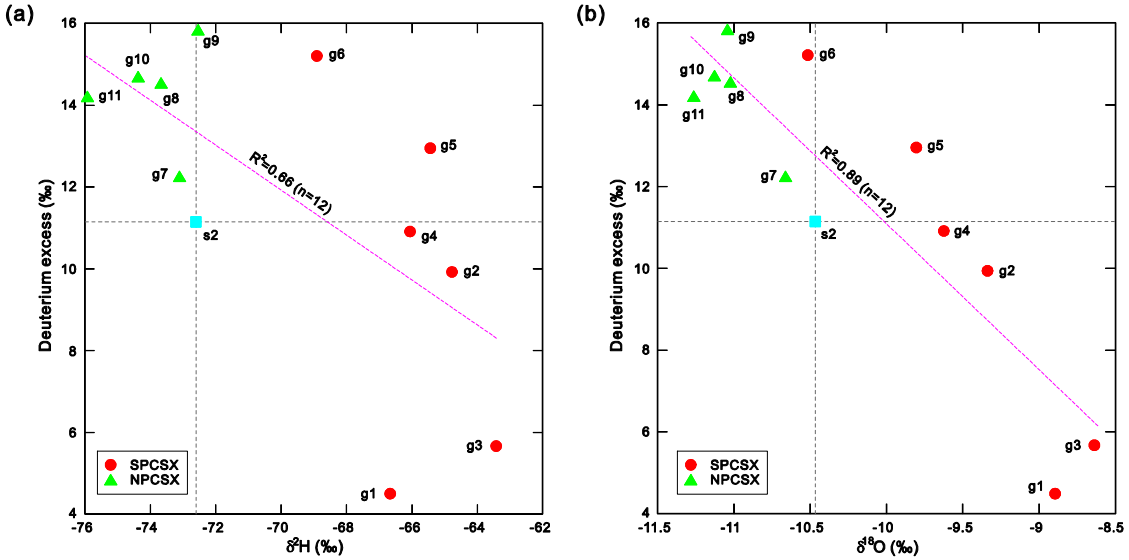

Figure 12. The bivariate plots of δ^2H (**a**) and $\delta^{18}O$ (**b**) vs. the deuterium excess for the groundwaters in the PCSX area. "PCSX" is a palaeochannel named in this study, with the north part of the channel named "NPCSX" and the south part named "SPCSX".

In addition to stable isotopes, the tritium contents were broadly and positively related to the values of deuterium excess in the groundwater samples in the PCSX section (Figure 13a). Except for sample g11 (a sample very close to the riverhead area), the positive relationship between the tritium and the deuterium excess generally shows that the d-excess values are higher in the groundwaters collected from the NPCSX, but are lower in those from the SPCSX (Figure 13a). This distribution pattern indicates that the groundwaters in the NPCSX are relatively younger and experienced a lower degree of evaporation than those in the SPCSX. The d-excess gradient, increasing from south to north in the PCSX, further confirms that groundwater does not flow from the SPCSX area to the NPCSX area.

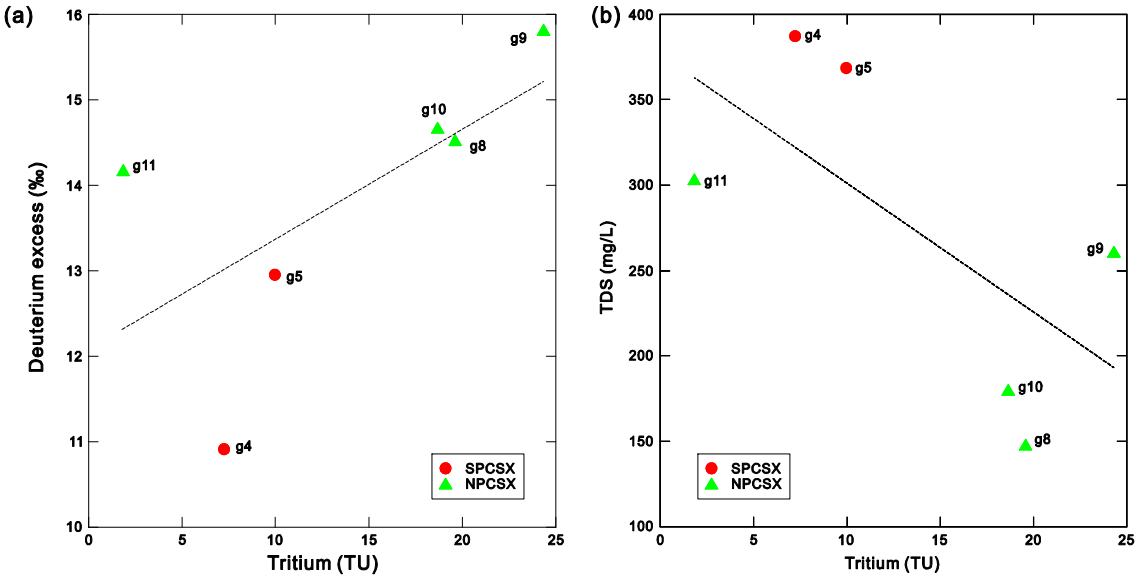

Figure 13. The variations of tritium contents vs. deuterium excess (**a**) and TDS (**b**) for the groundwater samples in the study area.

In Figure 13b, the tritium contents of groundwater increase while the TDS decreases from south to north in the PCSX (Figure 13b). This distribution pattern of the two environmental tracers further proved that the groundwaters in the NPCSX are younger and fresher than those in the SPCSX.

The reason why the older groundwater has a higher TDS value can be attributed to the fact that most minerals dissolve slowly in an aquifer and the older groundwater stays in contact with the surrounding rocks for a longer time allowing more minerals to pass in solution into the water, leading to a higher TDS [56]. Many studies (e.g., References [57,58] have demonstrated that groundwater flows in the direction in which it gets older. In view of this point, groundwaters in the PCSX region should theoretically flow from the NPCSX area to the SPCSX area, in opposition to the S-N topographical gradient in the PCSX region.

According to the speculation of mountains waters in colder and wetter conditions as mentioned above, it can be assumed that groundwaters in the HSDK Desert are recharged from remote mountain areas (about 150–200 km to the east and southeast) but not from the north neighboring catchment.

5.5. Groundwater Recharge in Desert Regions and Its Environmental Significance

Many studies showed that rainfall below 200 mm usually results in vulnerable recharge, thus we focused primarily on global semiarid and arid regions [11,59–65]. These studies proposed that the importance of local recharge mechanism should be considered in developing regional recharge estimates for water resource assessment in these areas. With regard to a continental view on groundwater recharge sourced from precipitation (diffusion recharge) in global semiarid and arid regions, average recharge rates estimated over large areas range from 0.2 to 35 mm/year (e.g., Reference [10]), representing only 0.1 to 5% of long-term average annual precipitation. This means that the average recharge is globally low for the arid lands. In this study, however, the recharge sources of groundwater deduced from the hydrochemical and isotopic analyses mainly come from remote mountain areas, but not from local or regional precipitation, thus, the focused recharge is significant than the diffusion recharge for this desert. Globally speaking, focused recharge and preferential flow usually result in highly variable recharge rates in semiarid and arid regions [10], even up to 720 m/year. Based on the analytical results in this study it was discovered that the groundwaters studied are fresh and young and that no Cl-type and Na-type waters occur in the study area (Figure 6). Additionally, because of the fact that the two rivers originate from the eastern HSDK Desert, one can conclude that the recharge rate of groundwater in the HSDK Desert is very high.

An important question between groundwater and its related environment in arid regions is how climate variability or climate change will influence groundwater recharge. Recharge research evaluated in this study indicates that the summer and winter precipitation related to the East Asian Monsoon (EAM) climate should not alter recharge in the HSDK Desert because linkages between the groundwater recharge and the modern and palaeo-atmospheric precipitation in this desert are weak. In contrast, elevated remote mountain precipitation enhances the stream's flow in the surrounding regions, which results in focused recharge beneath streams in the desert regions. Therefore, monitoring the stream's flow and flash floods coming from highlands such as the Daxing'Anling and north Yinshan Mountains related to EAM can be used to predict the impacts of climate on groundwater recharge in the HSDK Desert. However, the effects of geology and the distribution of hydraulic properties on the movement of water through thick unsaturated zones are not well understood in global arid regions, particularly in the HSDK Desert.

6. Conclusions

Few datums are related to the groundwater recharge and its origin are available for the HSDK desert, a region that is under the influence of the East Asian Summer Monsoon (EASM) climate. In this study, chemical, stable and radioactive isotopic (hydrogen and oxygen) characteristics of shallow groundwater, river water, spring water, lake water and local precipitation in the HSDK Desert and neighboring areas were investigated to reveal the relationships between various water bodies and the origin of groundwater. Isotopic and hydrogeochemical results show that (1) the natural waters studied are freshwater (TDS < 1000 mg/L) and there are no Cl-type and Na-type waters occurring in the desert, (2) the groundwaters, river waters, and spring waters are depleted in δ^2H and $\delta^{18}O$ compared with

modern precipitation, suggesting that the groundwaters are derived from cold water different from the local EASM precipitation, (3) the high contents (5–25 TU) of tritium in the groundwaters indicate that they are young and are not recharged by fossil waters formed during the past glacial periods, (4) groundwaters in the desert are recharged from remote mountain areas but not from the neighboring catchment (Dali Basin), (5) the focused recharge is significant for this desert with a high recharge rate of groundwater, and monitoring stream flow and flash floods coming from highlands related to EAM can be used to predict the impact of climate on groundwater recharge in the HSDK Desert.

Supplementary Materials: The following are available online at http://www.mdpi.com/2073-4441/10/11/1515/s1, Table S1: The physical parameters measured for the natural water samples in the study area, Table S2: The concentrations of major cations and anions measured for the water samples in the study area.

Author Contributions: For research articles with several authors, a short paragraph specifying their individual contributions must be provided. The following statements should be used "Conceptualization, B.-Q.Z., X.-Z.R. and P.R.; Methodology, B.-Q.Z. and X.-Z.R.; Software, B.-Q.Z. and X.-Z.R.; Validation, B.-Q.Z., X.-Z.R. and P.R.; Formal Analysis, B.-Q.Z. and X.-Z.R.; Investigation, B.-Q.Z. and X.-Z.R.; Resources, B.-Q.Z. and X.-Z.R.; Data Curation, B.-Q.Z. and X.-Z.R.; Writing-Original Draft Preparation, B.-Q.Z., X.-Z.R. and P.R.; Writing-Review & Editing, B.-Q.Z., X.-Z.R. and P.R.; Visualization, B.-Q.Z. and X.-Z.R.; Supervision, B.-Q.Z.; Project Administration, B.-Q.Z. and X.-Z.R.; Funding Acquisition, B.-Q.Z. and X.-Z.R.", please turn to the CRediT taxonomy for the term explanation. Authorship must be limited to those who have contributed substantially to the work reported.

Funding: This study was financially supported by the National Natural Science Foundation of China (41771014), the National Key Research and Development Program of China (2016YFA0601900) and the National Natural Science Foundation of China (41602196).

Acknowledgments: We thank the China Meteorological Data Sharing Service system for providing the weather data. Sincere thanks are also extended to Xiaoping Yang and other workmates for their generous help in the research work.

Conflicts of Interest: The authors declare no conflict of interest.

References

1. Alley, W.M.; Healy, R.W.; LaBaugh, J.W.; Reilly, T.E. Flow and storage in groundwater systems. *Science* **2002**, *296*, 1985–1990. [CrossRef] [PubMed]
2. Weissmann, G.S.; Zhang, Y.; LaBolle, E.M.; Fogg, G.E. Dispersion of groundwater age in an alluvial aquifer system. *Water Resour. Res.* **2002**, *38*, 1198. [CrossRef]
3. Sturchio, N.C.; Du, X.; Purtschert, R.; Lehmann, B.E.; Sultan, M.; Patterson, L.J.; Lu, Z.T.; Muller, P.; Bigler, T.; Bailey, K.; et al. One million year old groundwater in the Sahara revealed by krypton-81 and chlorine-36. *Geophys. Res. Lett.* **2004**, *31*, L05503. [CrossRef]
4. Bethke, C.M.; Johnson, T.M. Groundwater age and groundwater age dating. *Annu. Rev. Earth Planet. Sci.* **2008**, *36*, 121–152. [CrossRef]
5. McCallum, J.L.; Cook, P.G.; Simmons, C.T. Limitations of the use of environmental tracers to infer groundwater age. *Groundwater* **2014**, *53*, 56–70. [CrossRef] [PubMed]
6. Gleeson, T.; Befus, K.M.; Jasechko, S.; Luijendijk, E.; Cardenas, M.B. The global volume and distribution of modern groundwater. *Nat. Geosci.* **2016**, *9*, 161–167. [CrossRef]
7. Foster, S.S.D.; Chilton, P.J. Groundwater: The processes and global significance of aquifer degradation. *Philos. Trans. R. Soc. Lond. B* **2003**, *358*, 1957–1972. [CrossRef] [PubMed]
8. Taylor, R.G.; Scanlon, B.; Doll, P.; Rodell, M.; Beek, R.V.; Wada, Y.; Longuevergne, L.; Leblanc, M.; Famiglietti, J.S.; Edmunds, M.; et al. Ground water and climate change. *Nat. Clim. Chang.* **2013**, *3*, 322–329. [CrossRef]
9. Moore, W.S. Large groundwater inputs to coastal waters revealed by 226Ra enrichments. *Nature* **1996**, *380*, 612–614. [CrossRef]
10. Scanlon, B.R.; Keese, K.E.; Flint, A.L.; Flint, L.E.; Gaye, C.B.; Edmunds, W.M.; Simmers, I. Global synthesis of groundwater recharge in semiarid and arid regions. *Hydrol. Processes* **2006**, *20*, 3335–3370. [CrossRef]
11. Lerner, D.N.; Issar, A.S.; Simmers, I. *Groundwater Recharge. A Guide to Understanding and Estimating Natural Recharge*; Heinz Heise: Hanover, Germany, 1990; Volume 8, 345p.
12. Sorman, A.U.; Abdulrazzak, M.J.; Morel-Seytoux, H.J. Groundwater recharge estimation from ephemeral streams. Case study: Wadi Tabalah, Saudi Arabia. *Hydrol. Processes* **1997**, *11*, 1607–1619. [CrossRef]

13. De Vries, J.J.; Simmers, I. Groundwater recharge: An overview of processes and challenges. *Hydrogeol. J.* **2002**, *10*, 5–17. [CrossRef]
14. Chen, F.; Chen, J.; Holmes, J.; Boomer, I.; Austin, P.; Gates, J.B.; Wang, N.; Brooks, S.J.; Zhang, J. Moisture changes over the last millennium in arid central Asia: A review, synthesis and comparison with monsoon region. *Quat. Sci. Rev.* **2010**, *29*, 1055–1068. [CrossRef]
15. Yang, X.; Scuderi, L.A.; Wang, X.; Scuderi, L.J.; Zhang, D.; Li, H.; Forman, S.; Xu, Q.; Wang, R.; Huang, W.; et al. Groundwater sapping as the cause of irreversible desertification of Hunshandake Sandy Lands, Inner Mongolia, Northern China. *Proc. Natl. Acad. Sci. USA* **2015**, *112*, 702–706. [CrossRef] [PubMed]
16. Eizenhöfer, P.R.; Zhao, G.; Zhang, J.; Sun, M. Final closure of the Paleo-Asian Ocean along the Solonker Suture Zone: Constraints from geochronological and geochemical data of Permian volcanic and sedimentary rocks. *Tectonics* **2014**, *33*, 441–463. [CrossRef]
17. Lu, H.Y.; Miao, X.D.; Zhou, Y.L.; Mason, J.; Swinehart, J.; Zhang, J.F.; Zhou, L.P.; Yi, S.W. Late Quaternary aeolian activity in the Mu Us and Otindag dune fields (north China) and lagged response to insolation forcing. *Geophys. Res. Lett.* **2005**, *32*, 2465–2475. [CrossRef]
18. Gong, Z.J.; Li, S.H.; Sun, J.M.; Xue, L. Environmental changes in Hunshandake (Otindag) sandy land revealed by optical dating and multi-proxy study of dune sands. *J. Asian Earth Sci.* **2013**, *76*, 30–36. [CrossRef]
19. Ge, X.; Li, Y.; Luloff, A.E.; Dong, K.; Xiao, J. Effect of agricultural economic growth on sandy desertification in Horqin Sandy Land. *Ecol. Econ.* **2015**, *119*, 53–63. [CrossRef]
20. Zhu, Z.; Wu, Z.; Liu, S.; Di, X. *An Outline of Chinese Deserts*; Science Press: Beijing, China, 1980. (In Chinese)
21. Yang, X.; Zhu, B.; Wang, X.; Li, C.; Zhou, Z.; Chen, J.; Yin, J.; Lu, Y. Late Quaternary environmental changes and organic carbon density in the Hunshandake Sandy Land, eastern Inner Mongolia, China. *Glob. Planet. Chang.* **2008**, *61*, 70–78. [CrossRef]
22. Jian, P.; Liu, D.; Kröner, A.; Windley, B.F.; Shi, Y.; Zhang, W.; Zhang, F.; Miao, L.; Zhang, L.; Tomurhuu, D. Evolution of a Permian intraoceanic arc-trench system in the Solonker suture zone, Central Asian Orogenic Belt, China and Mongolia. *Lithos* **2010**, *118*, 169–190. [CrossRef]
23. Zhang, Z.; Li, K.; Li, J.; Tang, W.; Chen, Y.; Luo, Z. Geochronology and geochemistry of the Eastern Erenhot ophiolitic complex: Implications for the tectonic evolution of the Inner Mongolia–Daxinganling Orogenic Belt. *J. Asian Earth Sci.* **2015**, *97*, 279–293. [CrossRef]
24. Jahn, B.M. The Central Asian Orogenic Belt and growth of the continental crust in the Phanerozoic. *Geol. Soc. Lond. Spec. Publ.* **2004**, *226*, 73–100. [CrossRef]
25. Wang, Q.; Liu, X.Y. Paleoplate tectonics between Cathaysia and Angaraland in Inner Mongolia of China. *Tectonics* **1986**, *5*, 1073–1088. [CrossRef]
26. Li, J.Y. Permian geodynamic setting of Northeast China and adjacent regions: Closure of the Paleo-Asian Ocean and subduction of the Paleo-Pacific Plate. *J. Asian Earth Sci.* **2006**, *26*, 207–224. [CrossRef]
27. Li, S.; Sun, W.; Li, X.; Zhang, B. Sedimentary characteristics and environmental evolution of Otindag sandy land in Holocene. *J. Desert Res.* **1995**, *15*, 323–331. (In Chinese)
28. Peel, M.C.; Finlayson, B.L.; Mcmahon, T.A. Updated world map of the Koppen-Geiger climate classification. *Hydrol. Earth Syst. Sci.* **2007**, *11*, 1633–1644. [CrossRef]
29. Tian, F.; Wang, Y.; Liu, J.; Tang, W.K.; Jiang, N. Late Holocene climate change inferred from a lacustrine sedimentary sequence in southern Inner Mongolia, China. *Quat. Int.* **2017**, *452*, 22–32. [CrossRef]
30. Li, J.Y.; Xu, B.; Yang, X.C.; Jin, Y.X.; Li, Y.Y.; Zhang, J.; Zhao, L.N.; Li, R.L. Dynamic changes and driving force of grassland sandy desertification in Xilin Gol: A case study of Zhenglan Banner. *Geogr. Res.* **2011**, *9*, 1669–1682.
31. Wu, J.; An, N.; Ji, Y.; Wei, X. Analysis on Characteristics of Precipitation and Runoff in Silas MuLun River Basin. *Meteorol. J. Inner Mong.* **2014**, *4*, 23–25. (In Chinese)
32. Yao, S.; Zhu, Z.; Zhang, S.; Zhang, S.; Li, Y. Using SWAT model to simulate the discharge of the river Shandianhe in Inner Mongolia. *J. Arid Land Resour. Environ.* **2013**, *27*, 175–180. (In Chinese)
33. Gran, G. Determination of the equivalence point in potentiometric titrations. Part II. *Analyst* **1952**, *77*, 661–671. [CrossRef]
34. Meybeck, M. Global occurrence of major elements in rivers. In *Surface and Ground Water, Weathering, and Soils*; Drever, J.I., Holland, H.D., Turekian, K.K., Eds.; Treatise on Geochemistry; Elsevier-Pergamon: Oxford, UK, 2004; Volume 5, pp. 207–223.

35. Schoeller, H. *Géochemie Des Eaux Souterraines: Application Aux Eaux Des Gisements De Pétrole*; Société des éditions Technip: Paris, France, 1955.
36. Zhu, B.Q.; Yang, X.P.; Rioual, P.; Qin, X.G.; Liu, Z.T.; Xiong, H.G.; Yu, J.J. Hydrogeochemistry of three watersheds (the Erlqis, Zhungarer and Yili) in northern Xinjiang, NW China. *Appl. Geochem.* **2011**, *26*, 1535–1548. [CrossRef]
37. Zhu, B.Q.; Yu, J.J.; Qin, X.G.; Rioual, P.; Xiong, H.G. Climatic and geological factors contributing to the natural water chemistry in an arid environment from watersheds in northern Xinjiang, China. *Geomorphology* **2012**, *153–154*, 102–114. [CrossRef]
38. Clark, I.D. *Groundwater Geochemistry and Isotopes*; CRC Press: Boca Raton, FL, USA, 2015.
39. Piper, A.M. A graphic procedure in the geochemical interpretation of water-analyses. *Trans. Am. Geophys. Union* **1944**, *25*, 914–928. [CrossRef]
40. Craig, H. Isotopic Variations in Meteoric Waters. *Science* **1961**, *133*, 1702–1703. [CrossRef] [PubMed]
41. Stolp, B.J.; Solomon, D.K.; Suckow, A.; Vitvar, T.; Rank, D.; Aggarwal, P.K.; Han, L.F. Age dating base flow at springs and gaining streams using helium-3 and tritium: Fischa-Dagnitz system, southern Vienna Basin, Austria. *Water Resour. Res.* **2010**, *46*, W07503. [CrossRef]
42. Chen, J.; Sun, X.; Gu, W.; Tan, H.; Rao, W.; Dong, H.; Liu, X.; Su, Z. Isotopic and hydrochemical data to restrict the origin of the groundwater in the Badain Jaran Desert, Northern China. *Geochem. Int.* **2012**, *50*, 455–465. [CrossRef]
43. Yang, X.; Wang, X.; Liu, Z.; Li, H.; Ren, X.; Zhang, D.; Ma, Z.; Rioual, P.; Jin, X.; Scuderi, L. Initiation and variation of the dune fields in semi-arid China—With a special reference to the Hunshandake Sandy Land, Inner Mongolia. *Quat. Sci. Rev.* **2013**, *78*, 369–380. [CrossRef]
44. Gat, J.R.; Issar, A. Desert isotope hydrology: Water sources of the Sinai Desert. *Geochim. Cosmochim. Acta* **1974**, *38*, 1117–1131. [CrossRef]
45. Gat, J.R. Precipitation, groundwater and surface waters: Control of climate parameters on their isotopic composition and their utilization as palaeoclimatological tools. In *Palaeoclimates and Palaeowaters: A Collection of Environmental Isotope Studies, Proceedings of the Advisory Group Meeting, Vienna, Austria, 25–28 November 1980*; IAEA: Vienna, Austria, 1983; pp. 3–12.
46. Love, A.J.; Herczeg, A.L.; Leaney, F.W.; Stadter, M.H.; Dighton, J.C.; Armstrong, D. Groundwater residence time and palaeohydrology in the Otway Basin, South Australia. *J. Hydrol.* **1994**, *153*, 157–187. [CrossRef]
47. Love, A.J.; Herczeg, A.L.; Sampson, L.; Cresswell, R.G.; Fifield, L.K. Sources of chloride and implications for 36Cl dating of old groundwater, south-western Great Artesian basin, Australia. *Water Resour. Res.* **2000**, *36*, 1561–1574. [CrossRef]
48. Zhao, L.; Xiao, H.; Dong, Z.; Xiao, S.; Zhou, M.; Cheng, G.; Yin, L.; Yin, Z. Origins of groundwater inferred from isotopic patterns of the Badain Jaran Desert, Northwestern China. *Groundwater* **2012**, *50*, 715–725. [CrossRef] [PubMed]
49. Ma, J.; Pan, F.; Chen, L.; Edmunds, W.M.; Ding, Z.; He, J.; Zhou, K.; Huang, T. Isotopic and geochemical evidence of recharge sources and water quality in the Quaternary aquifer beneath Jinchang city, NW China. *Appl. Geochem.* **2010**, *25*, 996–1007. [CrossRef]
50. Herreta, C.; Gamboa, C.; Custodio, E.; Jordan, T.; Godfrey, L.; Jodar, J.; Luque, J.A.; Vargas, J.; Saez, A. Groundwater origin and recharge in the hyperarid Cordillera de la Costa, Atacama Desert, northern Chile. *Sci. Total Environ.* **2018**, *624*, 114–132. [CrossRef] [PubMed]
51. Subyani, A.M. Use of chloride-mass balance and environmental isotopes for evaluation of groundwater recharge in the alluvial aquifer, Wadi Tharad, western Saudi Arabia. *Environ. Geol.* **2004**, *46*, 741–749. [CrossRef]
52. Guendouz, A.; Moulla, A.S.; Edmunds, W.M.; Zouari, K.; Shand, P.; Mamou, A. Hydrogeochemical and isotopic evolution of water in the Complexe Terminal aquifer in the Algerian Sahara. *Hydrogeol. J.* **2003**, *11*, 483–495. [CrossRef]
53. Herczeg, A.L.; Leaney, F. Review: Environmental tracers in arid-zone hydrology. *Hydrogeol. J.* **2011**, *19*, 17–29. [CrossRef]
54. Chen, J.; Yang, Q.; Hao, G. Using hydrochemical and environmental isotopical data to analyse groundwater recharge in the Hunshandake Sandy Land. *Inner Mong. Sci. Technol. Econ.* **2008**, *17*, 9–12. (In Chinese)

55. Zhen, Z.; Li, C.; Li, W.; Hu, Q.; Liu, X.; Liu, Z.; Yu, R. Characteristics of environmental isotopes of surface water and groundwater and their recharge relationships in Lake Dali basin. *J. Lake Sci.* **2014**, *26*, 916–922. (In Chinese)
56. Fitts, C.R. *Groundwater Science*; Academic Press: Amsterdam, The Netherlands, 2002.
57. Boronina, A.; Renard, P.; Balderer, W.; Stichler, W. Application of tritium in precipitation and in groundwater of the Kouris catchment (Cyprus) for description of the regional groundwater flow. *Appl. Geochem.* **2005**, *20*, 1292–1308. [CrossRef]
58. Kazemi, G.A.; Lehr, J.H.; Perrochet, P. *Groundwater Age*; John Wiley & Sons: Hoboken, NJ, USA, 2006.
59. Simmers, I. *Estimation of Natural Groundwater Recharge*; D. Reidel Publishing Co.: Boston, MA, USA, 1988; 510p.
60. Gee, G.W.; Hillel, D. Groundwater recharge in arid regions: Review and critique of estimation methods. *Hydrol. Processes* **1988**, *2*, 255–266. [CrossRef]
61. Sharma, M.L. *Groundwater Recharge*; Balkema, A.A., Ed.; A.A. Balkema Publishers: Rotterdam, The Netherlands, 1989; 323p.
62. Allison, G.B.; Gee, G.W.; Tyler, S.W. Vadose-Zone techniques for estimating groundwater recharge in arid and semiarid regions. *Soil Sci. Soc. Am. J.* **1994**, *58*, 6–14. [CrossRef]
63. IAEA. *Isotope Based Assessment of Groundwater Renewal in Water Scarce Regions*; IAEA-TECDOC-1246; IAEA: Vienna, Austria, 2001; 273p.
64. Scanlon, B.R.; Cook, P.G. Preface: Theme issue on groundwater recharge. *Hydrogeol. J.* **2002**, *10*, 3–4. [CrossRef]
65. Hogan, J.F.; Phillips, F.M.; Scanlon, B.R. *Groundwater Recharge in a Desert Environment: The Southwestern United States: Water Science Applications Series, Volume 9*; American Geophysical Union: Washington, DC, USA, 2004; 294p.